Q. Rev. Biophys. 11, 103-178.
Revzin, A., & von Hippel, P. H. (1977) Biochemistry 16, 4769-4776.
Riggs, A. D., Bourgeois, S., & Cohn, M. (1970) J. Mol. Biol. 53, 401-417.
Scatchard, G. (1949) Ann. N.Y. Acad. Sci. 51, 660-672.
Watanabe, F., & Schwarz, G. (1983) J. Mol. Biol. 163, 485-498.
Yamamoto, K. R., & Alberts, B. (1974) J. Biol. Chem. 249, 7076-7086.

Optical Detection of Triplet-State Magnetic Resonance Studies on Individual Tryptophan Residues of Serum Albumin: Correlation between Phosphorescence and Zero-Field Splittings†

Su-Yau Mao and August H. Maki*
Department of Chemistry, University of California, Davis. Davis, California 95616
Received October 6, 1986; Revised Manuscript Received January 9, 1987

ABSTRACT: Cyanogen bromide cleavage of bovine serum albumin (BSA) yields two fragments, N (1-183) and C (184-582), containing 183 and 399 amino acid residues, respectively. Each fragment contains one of the two Trp residues of BSA. The triplet-state properties of the Trp residues in each fragment are characterized in this study by phosphorescence and optically detected magnetic resonance spectroscopy, and the results are compared with those of the intact albumin. Trp-134 in fragment N is located in a hydrophobic environment in the interior of the protein, as reflected by its red-shifted phosphorescence and characteristic zero-field splittings. The spectral properties of Trp-212 in fragment C suggest its location in a partially buried, inhomogeneous environment. They show great similarity to those of human serum albumin, which contains a single Trp at position 214. The Trp phosphorescence 0,0-bands of fragments C and N are fitted with Gaussian functions by computer, and their relative contributions to the phosphoresence 0,0-band of BSA are adjusted to fit the observed BSA 0,0-band. The wavelength dependence of the $|D| - |E|$ transition frequencies of fragments N and C is then weighted by their 0,0-band intensity, taking into account differences in spin alignment, and summed to predict the peak frequency of the $|D| - |E|$ band profile as a function of phosphorescence wavelength for the intact BSA. Good agreement between predicted and observed behavior of $|D| - |E|$ vs. wavelength for the intact protein provides strong evidence for the additivity of the phosphorescence and ODMR spectra of the individual Trp sites in BSA. We find that Trp-134 and Trp-212 have wavelength-independent and wavelength-dependent zero-field splittings, respectively.

Albumin is the most abundant protein in mammalian plasma. The functional properties of serum albumin, other than its possible importance in maintenance of proper osmotic balance, relate to its unusual and versatile liganding ability. It binds such diversified substances as fatty acids, bilirubin, tryptophan, various metal ions, most anions, some hormones, and numerous drugs (Goldstein, 1949; Peters, 1975). The binding function is a means of transporting sparingly hydrosoluble substances between tissues or organs. Binding also serves an equally vital role in buffering or regulating the concentrations of various low molecular weight substances, since it is the concentration of unbound fatty acid, drug, and so on that is related to its physiological effect. Albumin has been a model protein for many and diverse physicochemical studies. It consists of a single polypeptide chain of about 580 residues and is cross-linked by 17 disulfide bridges. On the basis of sequence data (Brown, 1977), analysis of peptide fragments (Pederson & Foster, 1969; King, 1973), and hydrodynamic measurements (Weber, 1952; Yang & Foster, 1954; Harrington et al., 1956), albumin is proposed to have a domain-type structure (Pederson & Foster, 1969; Anderson & Weber, 1969; Brown, 1976). The three-dimensional model proposed by Brown and Shockley (1982) consists of three major domains, with each domain formed by two subdomains.

Spectroscopic analysis of the structural and binding properties of serum albumin with Trp as an intrinsic chromophore has been extensive (Zuclich et al., 1972; Fuller Noel & Hunter, 1972; Spector, 1975; Sklar et al., 1977; Berde et al., 1979; Bell & Brenner, 1982). Human serum albumin (HSA)[1] contains only one Trp residue at position 214; bovine serum albumin (BSA) has two Trp residues, at positions 134 and 212. This simplicity greatly enhances the usefulness of spectroscopic methods for studying the molecular mechanism of binding. HSA has the advantage for these types of studies that any event that causes a change in Trp spectra must be associated with a structural change in the region of the protein containing the single Trp residue. The interpretations for BSA are more complicated. The two Trp residues are probably not spectrally identical (Fuller Noel & Hunter, 1972; Burstein et al., 1973; Spector, 1975). The optical emission bands of excited Trp in proteins are generally broad even at 1.2 K due to a quasi-continuous distribution of environments at each site, and it is usually impossible to resolve the emission bands from Trp residues even in quite different regions of the protein molecule (von Schütz et al., 1974). Furthermore, the similarity between

† This work was partially supported by a National Science Foundation grant (A.H.M.) and by a UC Davis research award (S.-Y.M.).

[1] Abbreviations: BSA, bovine serum albumin; Cys, cystine; HSA, human serum albumin; Met, methionine; ODMR, optical detection of triplet-state magnetic resonance; SDS, sodium *n*-dodecyl sulfate; Trp, tryptophan; Tyr, tyrosine; zfs, zero-field splittings.

0006-2960/87/0426-3106$01.50/0

the general structural details of BSA and HSA (Brown, 1977) suggests that the common Trp residues are located in a similar environment, and therefore, they would have similar triplet-state properties. In our previous study of fatty acid binding to serum albumin (Mao & Maki, 1987), assignment of the Trp residues involved in BSA complexes with oleic acid was made on the basis of this assumption by comparison with the results obtained from oleic acid binding to HSA.

The present studies were made with the intention to understand better the spectral properties of individual Trp residues of BSA and their relationship to the overall spectral properties of BSA. Our approach consisted of degrading albumin into two fragments each containing a single Trp and an examination of the triplet-state parameters of each fragment separately. Cyanogen bromide cleavage at methionyl bonds was chosen, which yields only two large fragments, N (residues 1–183) and C (residues 184–582), retaining the domain-type structures (King & Spencer, 1970).

We have examined phosphorescence and optically detected magnetic resonance (ODMR) parameters of fragments N and C to characterize the individual triplet-state properties of the Trp residues at positions 134 and 212. ODMR spectroscopy in zero field has been applied to study protein structure for more than a decade (Kwiram, 1982; Maki, 1984). The excited triplet state of aromatic amino acid residues (of which Trp has been most extensively studied) is used as a spin probe whose magnetic resonance transitions can be detected with great sensitivity by optical methods. The zero-field splittings (zfs) are sensitive to the local environment (Zuclich et al., 1973). Furthermore, the correlations between the optical wavelength and the zfs parameters can provide information about emission from distinct Trp sites (von Schütz et al., 1974).

Here, we find the dependence of ODMR frequency on phosphorescence wavelength for fragments N and C of BSA. The results are weighted by the phosphorescence profile of each fragment, accounting for differences in spin alignment, and convoluted to give the peak frequency of the ODMR band as a function of wavelength for the intact BSA.

Materials and Methods

Materials. BSA and HSA, crystallized, lyophilized, and essentially fatty acid free (less than 0.005%), were obtained from Sigma and were used without further purification. SDS–polyacrylamide (15%) gel electrophoresis indicated that the albumins are free of impurities (less than 2%) as determined by Coomasie Brilliant Blue staining. Sephadex G-25 (50–150 μm) and Sephadex G-100 (40–120 μm) were also from Sigma. Ammonium formate, cyanogen bromide, L-cystine, 5,5′-dithiobis(2-nitrobenzoic acid), and formic acid were from Aldrich. A gel filtration calibration kit containing BSA (67 kDa), ovalbumin (43 kDa), chymotrypsinogen A (25 kDa), and ribonuclease A (13.7 kDa) and an electrophoresis calibration kit containing phosphorylase *b* (94 kDa), BSA (67 kDa), ovalbumin (43 kDa), carbonic anhydrase (30 kDa), soybean trypsin inhibitor (20.1 kDa), and α-lactalbumin (14.4 kDa) were from Pharmacia. Doubly distilled water and solvents of spectroscopic grade were used throughout the experiments. All other chemicals were of the purest quality available. Protein solutions were concentrated by use of Centricon (Amicon Co.) microconcentrators with a 10- or a 30-kDa molecular mass cut-off YM membrane.

Protein and peptide concentrations were determined from the absorbance at 280 nm with molar extinction coefficients of 4.0×10^4, 3.3×10^4, 2.2×10^4, and 1.8×10^4 M^{-1} cm^{-1} for BSA, HSA, fragment C, and fragment N, respectively. These were calculated from amino acid composition (Brown, 1977), with the extinction coefficients of Trp, Tyr, and Cys at 280 nm taken to be 5690, 1280, and 120 M^{-1} cm^{-1}, respectively (Edelhoch, 1967).

Preparation of BSA Fragments. Large fragments of BSA were obtained from cyanogen bromide cleavage, as described by King and Spencer (1970), with some modifications. Half-cystinyl BSA was first prepared to protect the free sulfhydryl group from reacting with cyanogen bromide. To a solution of BSA (156 mg, 2.2 μmol) in 5 mL of 0.1 M Tris (pH 7.96) was added a solution of L-cystine (3.37 mg, 14 μmol) in 7.1 mL of the same buffer. Because of the limited solubility of L-cystine, it was dissolved first in 0.1 mL of 1.08 N NaOH and then immediately diluted with 7 mL of buffer. After 17 h at 25 °C, the sulfhydryl titer had decreased from the initial value of about 0.64 mol/mol of BSA to less than 0.02 mol/mol, as determined by the Ellman procedure (Ellman, 1959). The BSA solution was desalted and concentrated to about 1.3 mL by ultrafiltration through a Centricon microconcentrator. To a 1.2-mL solution containing 1.33 μmol of salt-free BSA was added a solution of cyanogen bromide (294 mg, 2.772 mmol) in 3.6 mL of 98% formic acid. After 5 h at 25 °C, the excess reagents were removed by passage through a Sephadex G-25 column (1.5 × 16 cm). The column was eluted with a buffer of 0.174 M formic acid and 0.026 M ammonium formate (pH 2.86) at a flow rate of 35 mL/h. The front peak was collected. A 1-mL aliquot was next applied to a Sephadex G-100 column (1.5 × 49 cm) and eluted with the pH 2.86 ammonium formate buffer at a flow rate of 9 mL/h. Fractions of 0.46-mL volume were collected, and their absorbance at 280 nm was plotted vs. elution volume. Molecular weights of the materials contained in these bands were estimated by comparing the elution positions with those of standard proteins. Cuts containing homogeneous BSA, fragment N, and fragment C were determined by SDS–polyacrylamide (15%) gel electrophoresis. The fractions of the single component were pooled together and concentrated by ultrafiltration. The buffer was then exchanged into 20% (v/v) glycerol/aqueous 50 mM phosphate buffer, pH 7.4, for low-temperature spectroscopic measurements.

Extensive cleavage at Met-87 of fragment N was done by adding cyanogen bromide (1.3 mg, 12 μmol) in 150 μL of 98% formic acid into a 50-μL solution containing 40 nmol of fragment N. After 30 h at 25 °C, the reaction mixture was diluted 10-fold with water. Thus the concentration of formic acid is reduced far below the safety limit of the Centricon membrane. Excess reagents were then removed, and the buffer was exchanged into cryogenic solvent by ultrafiltration.

Phosphorescence and ODMR Spectra. Samples were contained in quartz tubes and inserted into a microwave slow-wave helix terminating a coaxial transmission line. This was then suspended in a dewar and chilled to 1.2 K by pumping on liquid helium. The sample was excited with a 100-W high-pressure Hg arc equipped with a 12-cm pathlength aqueous $NiSO_4$ (500 g/L) infrared filter. The excitation band centered at 295 nm was selected with a monochromator, using 4-nm band-pass to minimize tyrosine excitation. The phosphorescence at a right angle to the excitation path passed through a WG-345-2 glass filter and was collected by a 1-m monochromator (McPherson Model 2051) and detected by a cooled photomultiplier tube (EMI Model 9789QA). Data analysis was carried out on a Digital Pro-350 microcomputer interfaced with a 1024-channel signal averager (Nicolet Model 1072).

The phosphorescence spectra were measured with a 1.5-nm emission bandwidth at 4.2 K, and the 0,0-band was monitored

at its peak wavelength with a 3-nm band-pass for ODMR measurements. Microwaves were swept both with increasing and with decreasing frequency at the same rate of 30 MHz/s, and the peak frequencies were averaged to obtain the zero-field splittings. The swept frequencies were calibrated by a microwave frequency counter (Hewlett Packard Model 5351A). Wavelength-selected ODMR measurements were performed with a slit resolution of 1.0 or 1.2 nm. The $|D| - |E|$ transition was measured with microwaves scanned upward in frequency from 1.4 to 2.0 GHz at a rate of 17 MHz/s. Half of the difference in $|D| - |E|$ for sweeps made toward lower frequency was then subtracted from the measured frequencies to compensate for the fast-passage effect.

Fluorescence Measurements. Fluorescence measurements were performed on a Perkin-Elmer MPF-44B spectrofluorometer. Quenching experiments were made by exciting the samples at 280 nm, and the fluorescence intensity was monitored at the peak wavelength while aliquots of solution containing KI were added to the sample solution in the cuvette. The absorbance of peptide solutions at the exiting wavelength was never greater than 0.05. The fluorescence intensity was then corrected for the dilution, and a plot of F_0/F vs. $[I^-]$ was made according to the well-known Stern–Volmer (1919) law:

$$F_0/F = 1 + K_Q X \quad (1)$$

where F_0 and F are the fluorescence intensities without and with the quencher and X is the molar concentration of the quencher. Values of the collisional quenching constant K_Q were calculated from the slope of the plots.

In the case of a sample containing Trp side chains in different environments, the fluorescence does not follow the simple Stern–Volmer relationship. A modified Stern–Volmer relationship (Lehrer, 1971) is then used:

$$F_0/\Delta F = 1/(f_a K_Q X) + 1/f_a \quad (2)$$

where $\Delta F = F_0 - F$ and f_a is the fractional quenchable protein fluorescence. From eq 2, a plot of $F_0/\Delta F$ vs. $1/[I^-]$ will yield a straight line of slope $1/(f_a K_Q)$ and intercept $1/f_a$, with K_Q = intercept/slope.

RESULTS

Isolation of Cyanogen Bromide Fragments of BSA. It is known that BSA samples are mixtures in which about two-thirds of the molecules have a free cysteinyl residue (Hughes, 1947; Simpson & Saroff, 1958), but the remaining one-third has this cysteine in the form of a mixed disulfide with L-cysteine or glutathione (King, 1961). To avoid oxidation of the cysteine residue during cyanogen bromide cleavage, BSA was converted to the mixed-disulfide form by reaction with L-cystine (King & Spencer, 1970). Results of Ellman titration show that the sulfhydryl titer decreases from the initial value of about 0.64 mol/mol of BSA to less than 0.02 mol/mol after the conversion.

Cyanogen bromide cleavage of BSA may result in a maximum of five peptides, since BSA contains four methionine residues (Met-87, Met-183, Met-444, Met-546). However, the presence of cross-linking disulfide bonds between the peptides decreases the number of products to two (King & Spencer, 1970) as shown in Figure 1. The two products designated as fragment N (residues 1–183) and fragment C (residues 184–582) were isolated from the cleavage mixture by chromatography on Sephadex G-100 (Figure 2). The elution positions of fragments N and C indicated their molecular masses to be about 22 and 50 kDa, respectively. There was a significant amount of materials eluted in front of fragment C, which was identified as incompletely cleaved BSA,

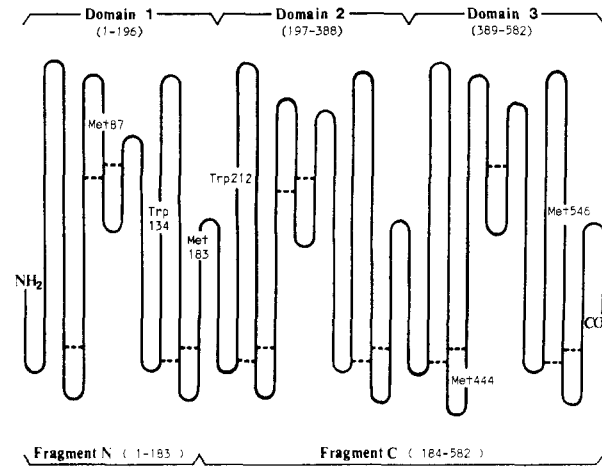

FIGURE 1: Schematic structure of BSA. The dashed lines indicate disulfide bridges. The positions of the two Trp and the four Met residues are indicated. Adapted from Brown and Shockley (1982).

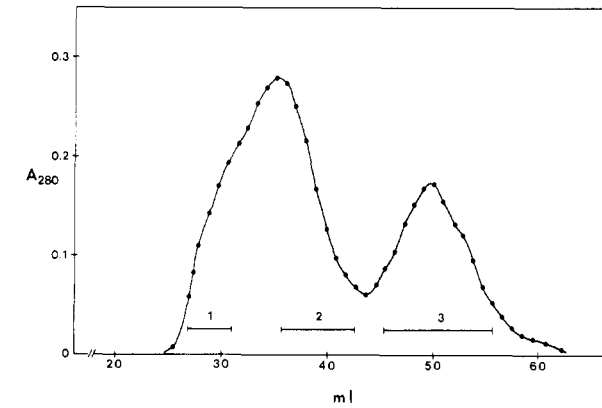

FIGURE 2: Separation of cyanogen bromide fragments of BSA on a Sephadex G-100 column (1.5 × 49 cm). The column was eluted with 0.174 M formic acid and 0.026 M ammonium formate (pH 2.86) at a flow rate of 9 mL/h, and fractions of 0.46-mL volume were collected. Cuts 1–3 contain incompletely cleaved BSA, fragment C, and fragment N, respectively.

since its elution position was close to that of intact BSA. The homogeneity of these fragments was studied by SDS–polyacrylamide gel electrophoresis. BSA (cut 1) and the fragments (cut 2 and 3) migrated as single bands, and the molecular masses were found to be 67, 47.3, and 19.5 kDa, respectively. The molar ratio of these products was estimated to be BSA:fragment N:fragment C = 1:3:3, which was calculated from the area under each peak in the elution profile.

Phosphorescence Spectroscopy. BSA contains two Trp residues, Trp-134 and Trp-212, whose 0,0-bands are not resolved. The phosphorescence 0,0-band occurs at 413.7 nm as a single peak (Figure 3), indicating that the two Trp residues are not located in very distinct environments. Figure 3 also shows the phosphorescence spectra of the two peptide fragments in comparison with that of intact BSA. Fragment C contains Trp-212, which is in homology with the lone Trp-214 of HSA according to the comparison of amino acid sequences of BSA and HSA (Brown, 1977). The 0,0-band of fragment C occurs at 412.5 nm and is in good agreement with that of HSA, which has its peak wavelength at 412.6 nm. This suggests that the two Trp residues have very similar environments and also is indicative that fragment C from BSA retains its structure in the vicinity of Trp-212 after cyanogen bromide cleavage. Since the 0,0-band of fragment C is blue shifted relative to that of BSA, it is interesting to ask whether fragment N containing Trp-134 has a red-shifted 0,0-band so

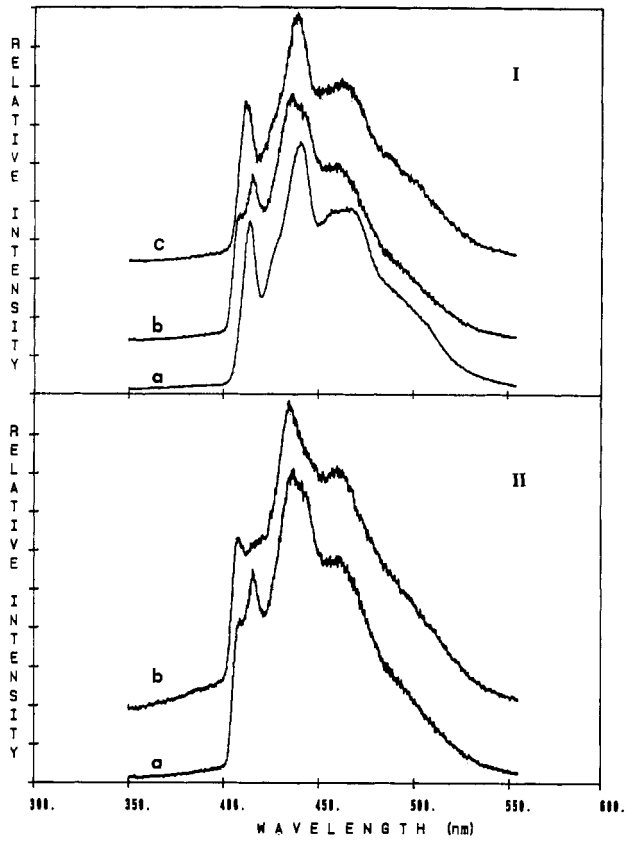

FIGURE 3: Phosphorescence spectra at 4.2 K of (Ia) BSA, (Ib) fragment N, (Ic) fragment C, (IIa) fragment N, and (IIb) fragment N′. The solvent is 20% glycerol/aqueous 50 mM phosphate buffer, pH 7.4. Sample concentrations are ca. 5×10^{-4} M. The excitation band is centered at 295 nm with 4-nm band-pass. The fragment N′ is prepared from fragment N by extensive cyanogen bromide digestion.

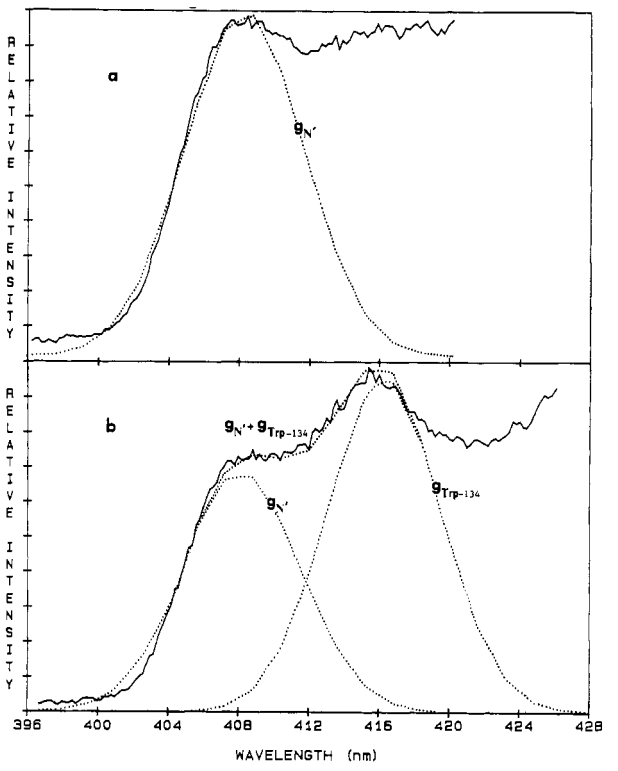

FIGURE 4: Deconvolution of the phosphorescence 0,0-band of fragment N. (a) 0,0-Band of fragment N′ and the fitted function $g_{N'}(\lambda)$. (b) 0,0-Band of fragment N and the fitted sum of $g_{N'}(\lambda) + g_{134}(\lambda)$, with relative contribution of $c_{N'}:c_{134} = 0.42:0.58$.

that the contributions from these two Trp residues yield the overall BSA phosphorescence spectrum. This is indeed the case; the 0,0-band of fragment N is red shifted by 2 nm relative to that of BSA and peaks at 415.7 nm (this is later corrected to be 416.3 nm by removing the contribution from molecules having a cleavage at Met-87), suggesting that Trp-134 is located in a hydrophobic environment. In addition to the major 0,0-band, a shoulder appears at the blue edge of the phosphorescence spectrum of fragment N (Figure 3Ib,IIa). Since there is only one Trp residue in this fragment, the inhomogeneous population is probably due to microheterogeneity in the environment of Trp; i.e., fractions of the sample have different conformations in the vicinity of Trp-134. One possibility is that some molecules are cleaved at Met-87 and may have an altered conformation, whereas some retain the intact structure. This possibility was investigated by carrying out extensive cyanogen bromide cleavage on fragment N; the sample thus prepared was designated as N′. The phosphorescence spectrum of this peptide is compared in Figure 3II with that of fragment N. The intensity of the blue shoulder increases and becomes a peak whose maximum occurs at 408.1 nm, while the 415.7-nm band is no longer resolved. This shows that the 408.1-nm band may be attributed to the molecules in which the peptide is cleaved at Met-87. The Trp probably becomes superficially located as suggested by the blue-shifted 0,0-band wavelength maximum. Therefore, the 415.7-nm band should be a reasonable representation of the 0,0-band of Trp-134 in the intact BSA. The 0,0-band of fragment N, containing heterogeneous Trp sites, was then deconvoluted to give the relative contributions from each Trp, as described in the following.

The phosphorescence 0,0-band of the nth Trp site is represented by a Gaussian line-shape function:

$$g_n(\lambda) = \exp[-\alpha_n^2(\lambda - \lambda_n)^2] \quad (3)$$

where $\alpha_n^2 = \ln 2/\Delta_n^2$ in which Δ_n is the half-width at half-intensity of the 0,0-band and λ_n is the peak wavelength of the 0,0-band. When there is more than one Trp site contributing to the emission of a peptide, the relative contribution from the nth Trp site is designated as c_n, where $\sum_n c_n = 1$. As shown in Figure 4a, the 0,0-band of fragment N′ was first fitted with a Gaussian function, $g_{N'}(\lambda) = \exp[-0.043(\lambda - 408.1)^2]$. A second Gaussian function, $g_{134}(\lambda)$, representing the 0,0-band of intact Trp-134 was next constructed with adjustable amplitude, bandwidth, and peak wavelength so that the sum of $g_{N'}(\lambda)$ and $g_{134}(\lambda)$ would best fit the 0,0-band of fragment N as shown in Figure 4b. We found that it is best fitted with $g_N(\lambda) = 0.42g_{N'}(\lambda) + 0.58g_{134}(\lambda)$, where $g_{134}(\lambda) = \exp[-0.048(\lambda - 416.3)^2]$.

Similar procedures were undertaken to deconvolute the 0,0-band of BSA. In Figure 5a, the 0,0-band of Trp-212 in fragment C was first fitted with a Gaussian function, $g_{212}(\lambda) = \exp[-0.034(\lambda - 412.5)^2]$. Figure 5b shows the Gaussian function, $g_{134}(\lambda)$, which was obtained earlier from the deconvolution of the fragment N 0,0-band (Figure 4b). The amplitudes of both $g_{212}(\lambda)$ and $g_{134}(\lambda)$ were then adjusted so that the sum of these two functions would best fit the 0,0-band of BSA. This is shown in Figure 5c, where $g_{BSA}(\lambda) = 0.55g_{212}(\lambda) + 0.45g_{134}(\lambda)$.

The phosphorescence spectrum was also measured on cut 1 from gel filtration, which contains incompletely cleaved BSA and thus can be used as a control. The 0,0-band occurs at 413.5 nm and is in good agreement with that of intact BSA (413.7 nm). This suggests that this protein fraction retains its conformation; little if any change in the microenvironment of Trp residues is observed.

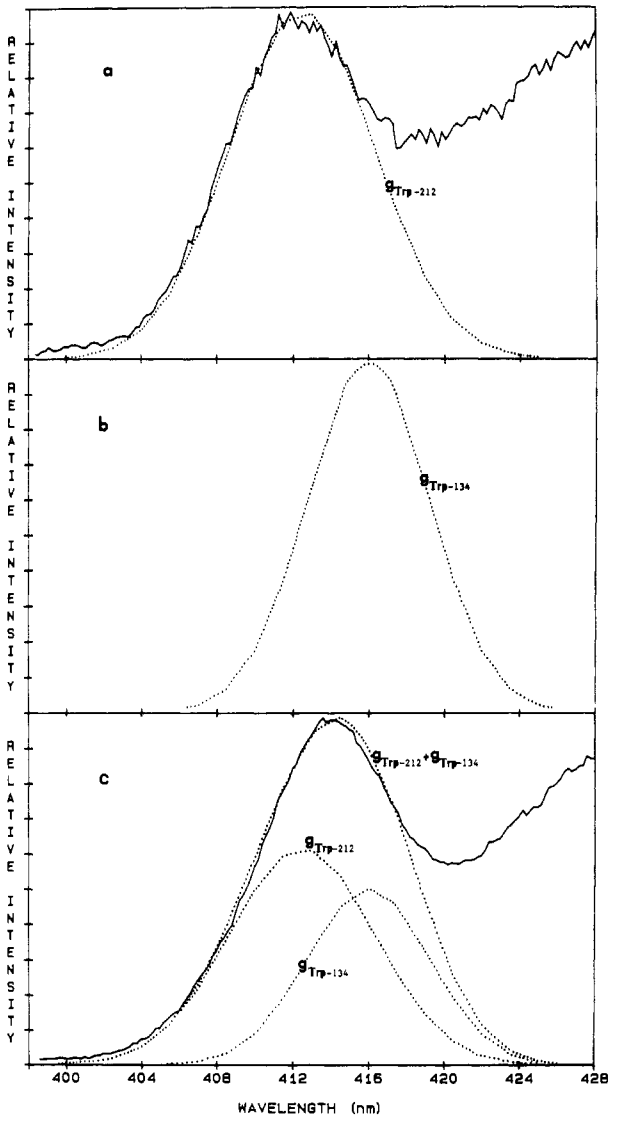

FIGURE 5: Deconvolution of the phosphorescence 0,0-band of BSA. (a) 0,0-Band of fragment C (Trp-212) and the fitted function $g_{212}(\lambda)$. (b) 0,0-Band of Trp-134 derived from deconvolution of the fragment N 0,0-band, described by $g_{134}(\lambda)$. (c) 0,0-Band of BSA and the fitted sum of $g_{212}(\lambda) + g_{134}(\lambda)$, with the relative contribution of $c_{212}:c_{134} = 0.55:0.45$.

Fluorescence Quenching. The heterogeneity in the Trp environment that exists in fragment N indicates that the conformation of some population of the peptide is different from that of the native protein. In order to find out the fraction of the populations having different conformations, fluorescence quenching studies were carried out on fragment N with iodide ions as the quencher. The collisional quenching constant (K_Q) for L-tryptophan was 11.8 M^{-1}, which is in good agreement with the value reported by Lehrer (1971). The quenching of the Trp fluorescence of fragments N and N′ by iodide is shown in Figures 6 and 7. Agreement with the simple Stern–Volmer relationship and the modified Stern–Volmer relationship is tested by plotting both F_0/F vs. $[I^-]$ (Figure 6) and $F_0/\Delta F$ vs. $1/[I^-]$ (Figure 7), respectively. Figure 6 shows a linear dependence obtained for fragment N′ where the peptide is cleaved at Met-87. This suggests a homogeneous population of the Trp side chains, which are subject to the same degree of fluorescence quenching.

The fluorescence of fragment N does not follow the simple Stern–Volmer relationship as judged by the nonlinear plot of Figure 6. Plotting the data according to the modified relationship (eq 2) resulted in a linear dependence as seen in Figure

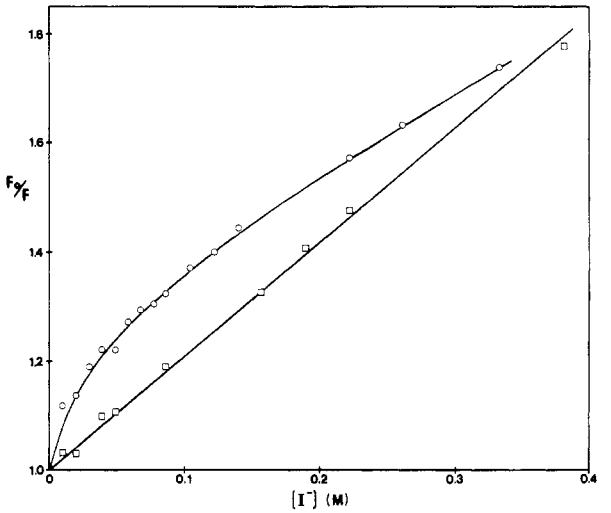

FIGURE 6: Stern–Volmer plot of the quenching of fragment N (○) and fragment N′ (□) fluorescence by iodide ions. The sample concentrations are ca. 1 μM. Excitation was performed at 280 nm (2-nm band-pass) and emission detected at 334 nm (5-nm band-pass).

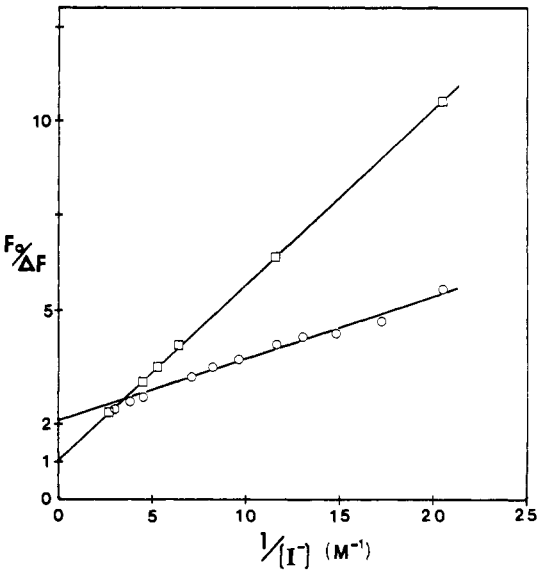

FIGURE 7: Modified Stern–Volmer plot of the quenching of fragment N (○) and fragment N′ (□) fluorescence by iodide. Conditions are given in Figure 6.

7. From the intercept a value of $f_a = 0.48$ was obtained. Thus, about 48% of the Trp fluorescence is accessible for quenching by iodide, and the other 52% is not affected by iodide in the concentration range 0–0.4 M. In contrast, the fluorescence of fragment N′ is completely accessible to iodide quenching as seen in Figure 7 by extrapolation to $f_a = 1$. Therefore, about 52% of the fragment N maintains an intact structure after cyanogen bromide cleavage, where the Trp-134 is buried in the interior of peptide. The remaining fraction has a cleavage at Met-87 that renders Trp-134 accessible to iodide ions.

ODMR Measurements. Table I lists the ODMR frequencies and zfs parameters for BSA, HSA, and the cyanogen bromide fragments of BSA. The zero-field splittings of BSA, $\nu_1 = 1.649$ GHz and $\nu_2 = 2.572$ GHz, together with the line widths, are similar to those for Trp located in a buried and hydrophobic protein environment (Figure 8Ia), whereas the ODMR signals of HSA suggest that the lone Trp residue is in a partially buried, relatively inhomogeneous region. The zfs parameters of the BSA sample that is isolated from the cyanogen bromide reaction also are compared with those of native BSA in Table I; the differences are within the exper-

Table I: ODMR Frequencies and zfs Parameters of BSA, HSA, and the Cyanogen Bromide Fragments of BSA

	$\lambda_{0,0}$ (nm)	ν_1 ($\Delta\nu$)[a]	ν_2 ($\Delta\nu$)[a]	D (GHz)	E (GHz)
BSA	413.7	1.649 (123)	2.572 (215)	2.935	1.286
HSA	412.6	1.684 (146)	2.539 (228)	2.953	1.269
BSA (cut 1)[b]	413.5	1.642 (134)	2.565 (244)	2.925	1.282
fragment C (cut 2)	412.5	1.684 (142)	2.552 (254)	2.960	1.276
fragment N (cut 3)	416.3	1.634 (121)	2.607 (223)	2.938	1.304
	408.1	1.743 (164)	2.419 (372)	2.953	1.210
fragment N'[c]	408.1	1.726 (191)	2.440 (395)	2.946	1.220

[a] Peak ODMR frequencies in GHz; the values given are the average of frequencies observed sweeping in both directions. The numbers in parentheses are line widths (fwhm) in MHz. [b] Incompletely cleaved BSA isolated from gel filtration. [c] Sample obtained from extensive cyanogen bromide digestion of fragment N.

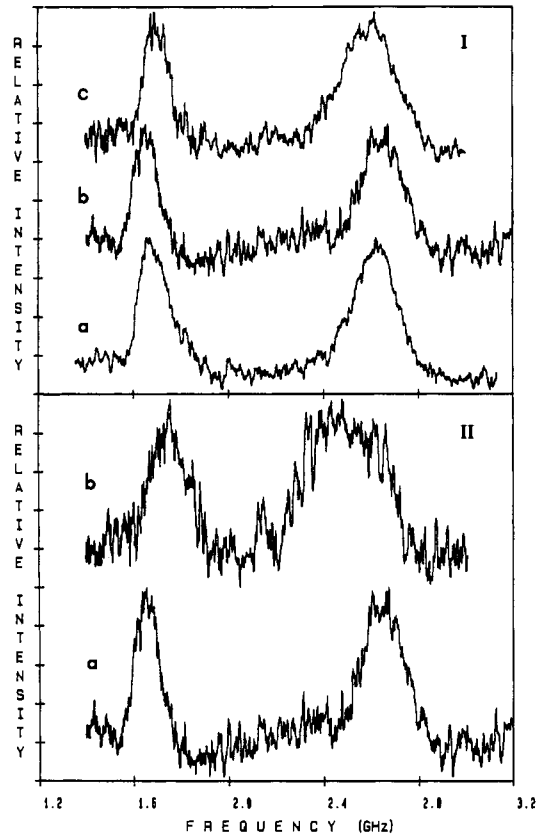

FIGURE 8: $|D| - |E|$ (low-frequency) and $2|E|$ (high-frequency) ODMR transitions of (Ia) BSA, (Ib) fragment N, (Ic) fragment C, (IIa) fragment N, and (IIb) fragment N'. The 0,0-band peak wavelengths that were monitored are given in Table I. In fragment N the 416.3-nm peak was monitored. Signal-averaged spectra (ca. 60 repetitions) shown are made with microwaves scanned from 1.4 to 3.0 GHz at a rate of 30 MHz/s.

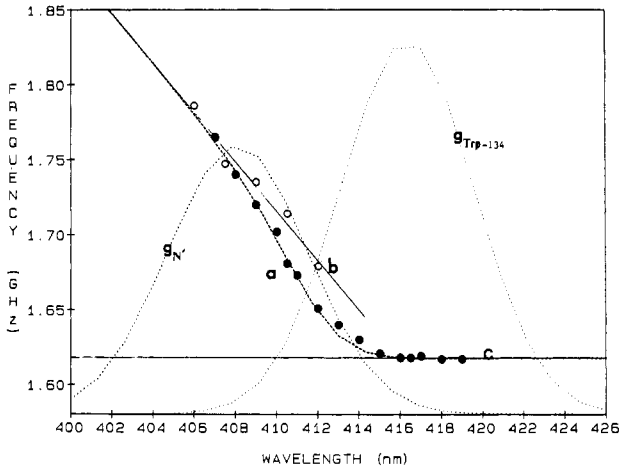

FIGURE 9: Variation in the $|D| - |E|$ transition frequency as a function of the emission wavelength for (a) fragment N (●), (b) fragment N' (○), and (c) Trp-134 of BSA [calculated profile, $f_{134}(\lambda) = 1.618$ GHz]. The emission band-pass was 1.0 nm for fragment N and 1.2 nm for fragment N'. The $|D| - |E|$ transition was measured with microwaves scanned up in frequency from 1.4 to 2.0 GHz at a rate of 17 MHz/s. The difference in $|D| - |E|$ for sweeps made toward lower frequency is 36 MHz on the average; the values shown in the graph have been corrected by subtracting 18 MHz from the measured peak frequencies. The 0,0-bands of fragment N' [$g_{N'}(\lambda)$] and Trp-134 [$g_{134}(\lambda)$] are also shown with the relative intensity given in Figure 4b. The dashed curve a is the convolution of curves b and c weighted by their respective spectral intensities.

imental precision of ±10 MHz. This is in line with the results obtained from phosphorescence measurements, indicating that the protein probably retains its conformation under the conditions of cyanogen bromide reaction and the series of isolation procedures.

The ODMR frequencies of fragment C, $\nu_1 = 1.684$ GHz and $\nu_2 = 2.552$ GHz (Figure 8Ib), are essentially the same as those of HSA. This provides further evidence that Trp-212 of BSA is homologous to the lone Trp-214 of HSA, and they are located in a similar environment in the protein.

The zfs of the two types of Trp present in the inhomogeneous fragment N preparation have quite different values. When monitoring the 416.3-nm band, we obtained $\nu_1 = 1.634$ GHz and $\nu_2 = 2.607$ GHz, both with relatively narrow line widths (Figure 8Ic). These frequencies are consistent with those for Trp located in a hydrophobic region; the narrow line widths indicate that Trp-134 is in a relatively homogeneous environment, i.e., the interior of the protein, whereas the ODMR signals of the blue-shifted band (408.1 nm) have the frequencies and line widths similar to those found for solvent-exposed Trp. After extensive cyanogen bromide digestion of fragment N, the ODMR measurements monitored at the only resolved 0,0-band (408.1 nm) indicate that the Trp residue becomes solvent-exposed when Met-87 is cleaved. The ODMR transitions of fragment N before and after cyanogen bromide digestion are compared in Figure 8II.

Wavelength-Selected ODMR. The $|D| - |E|$ transition frequencies of fragment N are plotted vs. wavelength in Figure 9 (curve a, filled circles). A change in slope occurs at about 413 nm and separates the signals into two sets, indicating that they originate from distinct Trp sites. The first set of signals vary linearly with wavelength, whereas the second set of signals are wavelength independent and are found in the red-shifted part of the 0,0-band. Figure 9b (open circles) shows the variation in the $|D| - |E|$ frequency with observing wavelength for fragment N', where Trp-134 becomes solvent exposed due to the cleavage at Met-87. A single set of signals appear at higher frequencies when monitored throughout the blue-shifted band (408.1 nm), with a monotonic and linear dependence on wavelength. This behavior is similar to the wavelength-dependent set of signals observed in fragment N (Figure 9a, filled circles). It has been shown that the red-shifted part of the 0,0-band of fragment N originates from the intact Trp-134 (Figure 4); therefore, the wavelength-independent set of signals

of fragment N may be attributed to Trp-134. In order to obtain the representation of the $|D| - |E|$ vs. wavelength behavior for Trp-134, deconvolution of curve a in Figure 9 (filled circles) is carried out as described in the following.

When there is more than one Trp site present, all contribute to the overall emission as well as to the ODMR transitions of the protein. Each Trp site has its own characteristic phosphorescence 0,0-band, $g_n(\lambda)$, and ODMR frequencies as a function of emission wavelength, which can be described by $f_n(\lambda)$. Assuming that the contribution from each Trp site to the ODMR transition frequency is proportional to its phosphorescence intensity at a given wavelength, then the observed ODMR transition frequency for the protein, $F(\lambda)$, would be the sum of the transition frequencies of individual Trp sites weighted by their relative phosphorescence intensity:

$$F(\lambda) = \sum_n c_n g_n(\lambda) f_n(\lambda) / \sum_n c_n g_n(\lambda) \quad (4)$$

This assumption is valid only if the extent of spin alignment in the triplet state is the same for the sites that contribute to the ODMR spectrum. For now we will assume this to be the case. The relative phosphorescence intensity of the nth Trp site, $g_n(\lambda)$, is obtained from the deconvolution of the overall phosphorescence 0,0-band given previously (Figures 4 and 5). For fragment N, the 0,0-bands of the two Trp sites with the relative contributions $c_{N'}:c_{134} = 0.42:0.58$ are also shown in Figure 9. The $|D| - |E|$ vs. wavelength plot for fragment N′ (Figure 9b, open circles) was first fitted with a linear function, $f_{N'}(\lambda) = -0.016467\lambda + 8.467$, while a wavelength-independent function, $f_{134}(\lambda)$ = constant, was used for the intact Trp-134 site, as judged by the wavelength-independent ODMR signals that appear in the red-shifted part of the 0,0-band. The value of the constant was adjusted so that the weighted sum, $F(\lambda)$ of eq 4, would best fit curve a (filled circles) in Figure 9. The best fit was obtained when $f_{134}(\lambda) = 1.618$ GHz (Figure 9, curve c), which in turn represents the behavior of $|D| - |E|$ vs. wavelength for the intact Trp-134. The excellent fitting of the wavelength-selected ODMR data for fragment N with the relative phosphorescence intensities as weighting factors for the intact and solvent-exposed sites supports the assumption made above that the spin alignment is the same for the two sites.

In Figure 10, the $|D| - |E|$ frequencies of fragment C are plotted as a function of the monitored wavelength (curve a, open circles). A single set of signals is observed, whose frequencies vary monotonically and approximately linearly with wavelength. This profile coincides with that found for HSA, providing further evidence that Trp-212 in fragment C is located in an environment very similar to that of the single Trp-214 in HSA. Figure 10b (filled circles) shows the dependence of the $|D| - |E|$ frequency on wavelength for BSA. In order to verify the relationship described by eq 4, convolution of the ODMR band profiles of Trp-212 and Trp-134 was carried out to predict that of the intact BSA. The $|D| - |E|$ vs. wavelength plot for Trp-212 in fragment C (Figure 10a, open circles) was first fitted with a function, $f_{212}(\lambda) = (4.065126 \times 10^{-4})\lambda^2 - 0.347213\lambda + 75.726$. The wavelength-independent function obtained from deconvolution of fragment N, $f_{134}(\lambda) = 1.618$ GHz (Figure 9c and Figure 10c), was used for Trp-134. Figure 10 also shows the 0,0-bands of Trp-134 and Trp-212, which are described by $g_{134}(\lambda)$ and $g_{212}(\lambda)$. The relative contributions from these two 0,0-bands were adjusted such that the resulting $F(\lambda)$ (eq 4) would best fit curve b in Figure 10 (filled circles). The relative contributions were found to be $c_{134}:c_{212} = 0.56:0.44$. The predicted curve (dashed line in Figure 10) is in good agreement with the experimental results (filled circles).

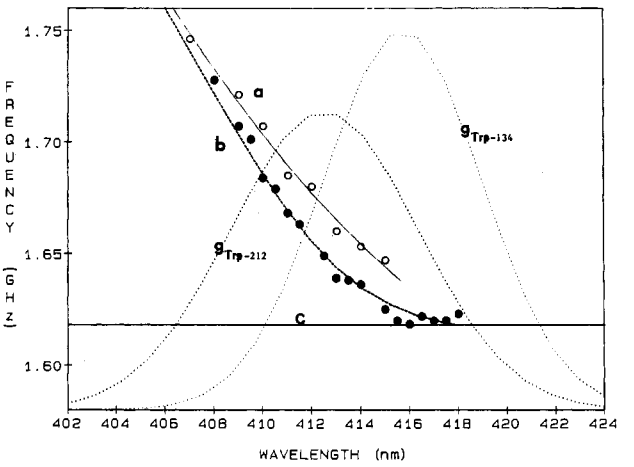

FIGURE 10: Wavelength dependence of the $|D| - |E|$ transition frequency of (a) fragment C (Trp-212) (○), (b) BSA (●), and (c) Trp-134 of BSA [calculated profile, $f_{134}(\lambda)$]. The emission band-pass was 1.2 nm for fragment C and 1.0 nm for BSA. The 0,0-bands of Trp-212 [$g_{212}(\lambda)$] and Trp-134 [$g_{134}(\lambda)$] shown are with the relative intensity of $c_{212}:c_{134} = 0.44:0.56$. The convoluted curve (dashed line) is compared with the experimental data (●) of BSA.

Discussion

The ODMR transition of aromatic molecules dissolved in aqueous glasses, which are most often used as solvents for biological molecules, are inhomogeneously broadened (Maki, 1984). The source of the inhomogeneous broadening is the interaction of the ensemble of molecules with the environment. It is observed generally that samples characterized by broad, inhomogeneously broadened optical transitions also are found to produce broad ODMR lines. The line-broadening phenomena are related (Lemaistre & Zewail, 1979; Zewail, 1979; Kwiram, 1982). A number of models for the primary mechanism of this broadening have been suggested, including the spin–orbit coupling models (Lemaistre & Zewail, 1979; Clark & Tinti, 1980) and the dipolar coupling model (van Egmond et al., 1975). These models each predict a linear correlation of the phosphorescence shift and the corresponding zfs shift. This correlation has been shown by both phosphorescence and zfs shifts induced by external electric fields (Clark & Tinti, 1980). The correlation has been observed also by monitoring the zfs as the emission wavelength is varied through the inhomogeneously broadened phosphorescence band (von Schütz et al., 1974; Kwiram et al., 1978; Gradl et al., 1986). If all of the Trp residues in a sample belong to the same set of environments as, for instance, in solvent-exposed Trp, a linear dependence of the zfs is obtained when the wavelength is varied through the 0,0-band. When the Trp phosphorescence of a protein containing Trp residues at more than one site is examined in a similar experiment, linear behavior is observed within a set, but discontinuities occur as the monitored wavelength passes from the emission of one set to that of another. Even if the 0,0-bands of the sets are not resolved optically, discontinuities in the zfs vs. wavelength plot may be interpreted as emissions from different Trp positions in the protein structure (von Schütz et al., 1974). This approach enabled us to assign a particular Trp residue of BSA that is involved in the complex formation with oleic acid in a previous study (Mao & Maki, 1987). When oleic acid is bound to BSA, the wavelength-independent curve of Trp-134 in BSA has vanished in the complex and is replaced by a new set of wavelength-dependent signals at shorter wavelength. It was concluded that Trp-134 in BSA is located near a primary

binding site for long-chain fatty acid and becomes greatly perturbed upon oleate binding.

Even though the optical spectrum of BSA provides no resolution of emission from individual residues, wavelength-selected ODMR measurements make it possible to distinguish between Trp residues. The dependence of the $|D| - |E|$ transition on wavelength shows a break in slope in the region of the overlapping 0,0-bands; a systematic reduction in the $|D| - |E|$ frequency with increasing wavelength occurs throughout the blue region but levels off toward the red edge of the 0,0-band. On the other hand, the single Trp-214 in HSA shows a monotonic and approximately linear dependence of the $|D| - |E|$ frequency on emission wavelength. This is similar to that observed for the wavelength-dependent set of signals in BSA, which appear in the blue region of the BSA 0,0-band. Therefore, the comparison between BSA and HSA suggests that the blue region of the BSA 0,0-band and the wavelength-dependent $|D| - |E|$ transitions are attributed to the common Trp residue at position 212, whereas the red edge of the BSA 0,0-band and the wavelength-independent $|D| - |E|$ transitions are attributed to Trp-134 in BSA.

We have studied the fragments of BSA produced by cyanogen bromide cleavage using ODMR spectroscopy in an attempt to further characterize the triplet states of individual Trp residues that are located in different positions on the protein chain, as well as to study their convolution to the zfs vs. wavelength profile of the intact protein. The two large fragments, N and C, are obtained by the cleavage at Met-183, which is located at the connecting segment between domain 1 and 2 according to the structural model proposed by Brown and Shockley (1982). Thus, fragments N and C correspond to one domain and two domains of the protein, respectively. It has been shown that the albumin fragments corresponding to domains retain their secondary structure and some of their binding properties (Reed et al., 1975; King & Spencer, 1970). In addition, the fragments, which are unfolded by reduction of their disulfide bonds, refold and regain antigenic specificity, indicating restoration of tertiary structure (Teale & Benjamin, 1976, 1977). Therefore, the conformations of fragment N and C are most likely to be the same as they are in the native protein. However, the other three methionine residues, Met-87, Met-444, and Met-546, which are located within domains, also are possibly accessible to cyanogen bromide cleavage. But cleavage at these three sites does not result in further degradation of the fragments due to the cross-linking disulfide bridges. The probability of cleavage at the Met-87 site is smaller than that for Met-183, since, although 75% of the BSA molecules are cleaved at Met-183, only 48% of the fragment N molecules (which are produced by the cleavage at Met-183) are cleaved at Met-87, as judged by the fluorescence quenching measurements. Both Met-444 and Met-546 are in domain 3. Thus, cleavage at these sites probably would not affect the protein conformation near Trp-212, which resides in domain 2. This is verified by the similarities of phosphorescence and ODMR spectra as well as of the zfs vs. λ profile between fragment C and HSA. On the other hand, for fragment N, the cleavage at Met-87 is more likely to alter the protein conformation in the vicinity of Trp-134 since they are located in the same domain. When the peptide chain is cleaved at Met-87 (fragment N′), Trp-134 becomes superficially located and thus accessible to quenching by iodide ions. The fragment N′ has lower intrinsic fluorescence intensity than fragment N (data not shown), which contains far more Trp-134 in its native environment. A possible explanation is that Trp-134 in fragment N′ has a lower quantum yield due to quenching by a nearby amino acid side chain after cleavage at Met-87. Measurements of the intrinsic fluorescence emission with excitation at 280 and 295 nm for both fragment N and fragment N′ show a lower 280/295 ratio for fragment N′. Since both Tyr and Trp are excited at 280 nm but only Trp is excited at 295 nm, the results imply that the cleavage at Met-87 renders the peptide chain more open. Thus, the energy transfer from Tyr residues to Trp is less effective.

The additivity of the phosphorescence and ODMR spectra of the individual Trp sittes in BSA has been demonstrated in this study. The relative contributions of the solvent-exposed Trp site and the buried Trp-134 site to the phosphorescence 0,0-band intensity of fragment N obtained from deconvolution of the 0,0-band are 0.42 and 0.58, respectively. These values are in good agreement with those obtained from fluorescence quenching measurements, where 48% of the emission is quenched by iodide ions and consequently is attributed to the solvent-exposed Trp site. Due to this heterogeneity in the phosphorescence emission of Trp in fragment N, the zfs vs. wavelength profile was first deconvoluted to obtain that of Trp-134 in the native protein structure. The profile thus obtained appears in the low-frequency region and is wavelength independent. On the other hand, the triplet-state properties of Trp-212 in BSA are characterized by studying fragment C. From the results obtained in this study, it is evident that the blue-shifted phosphorescence of BSA and the linearly wavelength-dependent $|D| - |E|$ transitions are from Trp-212; while the red edge of the BSA 0,0-band and the wavelength-independent zfs are attributed to Trp-134 in BSA. Each Trp site has characteristic phosphorescence and ODMR behavior and is weighted by its phosphorescence band contour in its contribution to the ODMR signal of the BSA. This is verified by the good agreement between the predicted ODMR band profile and the measured values. The differences are well within the experimental precision.

However, a discrepancy is found in the relative contribution of Trp-134 and Trp-212 to the phosphorescence 0,0-band intensity and $|D| - |E|$ transition frequency of BSA. The best fit to the 0,0-band of BSA was obtained with the relative contribution of $c_{134}:c_{212} = 0.45:0.55$ (Figure 5c). However, the relative contribution of Trp-134 and Trp-212 to the ODMR band profile of BSA resulting in the best fit to the experimental data was found to be $c_{134}:c_{212} = 0.56:0.44$. The most likely explanation for this discrepancy is the failure of our assumption that the spin alignment is the same for the two sites. The fitting of the wavelength-selected ODMR data for intact BSA demonstrates that the spin alignment of Trp-134 is higher than it is for Trp-212.

In this study, we have demonstrated that discontinuities occur in the zfs vs. monitored wavelength plot when the phosphorescence emission originates from distinct types of Trp sites. These discontinuities were attributed to the superposition of the magnetic resonance transitions associated with each of the emission components. Convolution of the Trp ODMR band profiles of the N and C fragments of BSA produced a good representation of the ODMR band profile of the intact protein. Thus, it was shown that Trp-134 and Tpr-212 of BSA have wavelength-independent and wavelength-dependent zfs parameters, respectively.

Registry No. Tryptophan, 73-22-3.

REFERENCES

Anderson, S. R., & Weber, G. (1969) *Biochemistry 8*, 371–377.

Bell, K. L., & Brenner, H. C. (1982) *Biochemistry 21*, 799–804.
Berde, C. B., Hudson, B. S., Simoni, R. D., & Sklar, L. A. (1979) *J. Biol. Chem. 254*, 391–400.
Brown, J. R. (1976) *Fed. Proc., Fed. Am. Soc. Exp. Biol. 35*, 2141–2144.
Brown, J. R. (1977) in *Albumin: Structure, Function, and Uses* (Rosenoer, V. M., Oratz, M., & Rothschild, M. A., Eds.) pp 27–51, Pergamon, Oxford.
Brown, J. R., & Shockley, P. (1982) in *Lipid-Protein Interactions* (Jost, P. C., & Griffith, O. H., Eds.) Vol. 1, pp 25–68, Wiley, New York.
Burstein, E. A., Vedenkina, N. S., & Ivkova, M. N. (1973) *Photochem. Photobiol. 18*, 263–279.
Clark, S. E., & Tinti, D. S. (1980) *Chem. Phys. 51*, 17–30.
Edelhoch, H. (1967) *Biochemistry 6*, 1948–1954.
Ellman, G. (1959) *Arch. Biochem. Biophys. 82*, 70–77.
Fuller Noel, J. K., & Hunter, J. J. (1972) *J. Biol. Chem. 247*, 7391–7406.
Goldstein, A. (1949) *Pharmacol. Rev. 1*, 102–165.
Gradl, G., Friedrich, J., & Kohler, B. E. (1986) *J. Chem. Phys. 84*, 2079–2083.
Harrington, W. F., Johnson, P., & Ottewill, R. H. (1956) *Biochem. J. 62*, 569–582.
Hughes, W. L. (1947) *J. Am. Chem. Soc. 69*, 1836–1837.
King, T. P. (1961) *J. Biol. Chem. 236*, PC5.
King, T. P. (1973) *Arch. Biochem. Biophys. 156*, 509–520.
King, T. P., & Spencer, M. (1970) *J. Biol. Chem. 245*, 6134–6148.
Kwiram, A. L. (1982) in *Triplet State ODMR Spectroscopy* (Clark, R. H., Ed.) pp 427–478, Wiley, New York.
Kwiram, A. L., Ross, J. B. A., & Deranleau, D. A. (1978) *Chem. Phys. Lett. 54*, 506–509.
Lehrer, S. S. (1971) *Biochemistry 10*, 3254–3263.
Lemaistre, J. P., & Zewail, A. H. (1979) *Chem. Phys. Lett. 68*, 296–301.
Maki, A. H. (1984) in *Biological Magnetic Resonance* (Berliner, L. J., & Reuben, J., Eds.) pp 187–294, Plenum, New York.
Mao, S. Y., & Maki, A. H. (1987) *Biochemistry* (in press).
Pederson, D. M., & Foster, J. F. (1969) *Biochemistry 8*, 2357–2365.
Peters, T. (1975) in *The Plasma Proteins* (Putnam, F. W., Ed.) Vol. 1, pp 133–181, Academic, New York.
Reed, R. G., Feldhoff, R. C., Clute, O. L., & Peters, T. (1975) *Biochemistry 14*, 4578–4583.
Simpson, R. B., & Saroff, H. A. (1958) *J. Am. Chem. Soc. 80*, 2129–2131.
Sklar, L. A., Hudson, B. S., & Simoni, R. D. (1977) *Biochemistry 16*, 5100–5108.
Spector, A. A. (1975) *J. Lipid Res. 16*, 165–179.
Stern, O., & Volmer, M. (1919) *Phys. Z. 20*, 183–188.
Teale, J. M., & Benjamin, D. C. (1976) *J. Biol. Chem. 251*, 4609–4615.
Teale, J. M., & Benjamin, D. C. (1977) *J. Biol. Chem. 252*, 4521–4526.
van Egmond, J., Kohler, B. E., & Chan, I. Y. (1975) *Chem. Phys. Lett. 34*, 423–426.
von Schütz, J. U., Zuclich, J., & Maki, A. H. (1974) *J. Am. Chem. Soc. 96*, 714–718.
Weber, G. (1952) *Biochem. J. 51*, 155–167.
Yang, J. T., & Foster, J. F. (1954) *J. Am. Chem. Soc. 76*, 1588–1595.
Zewail, A. H. (1979) *J. Chem. Phys. 70*, 5759–5766.
Zuclich, J., Schweitzer, D., & Maki, A. H. (1972) *Biochem. Biophys. Res. Commun. 46*, 1764–1768.
Zuclich, J., Schweitzer, D., & Maki, A. H. (1973) *Photochem. Photobiol. 18*, 161–168.